Advances in Science and Technology Research Journal

Advances in Science and Technology Research Journal, 2026, 20(10), 328–339
https://doi.org/10.12913/22998624/225487
ISSN 2299-8624, License CC-BY 4.0

Received: 2026.06.01
Accepted: 2026.07.15
Published: 2026.09.01

Integrated one-way aero-structural analysis of an aircraft wing using a MATLAB-based panel method and finite element analysis

Mohammed Kheiraldeen Abbas[1], Tarik Hassan Elsonni[2*], Mokdad Hayawi Rahman[2], Emad Qasem Hussein[3], Alnazir Khalafallah Alatta[4]

[1] Department of Mechanical Engineering, College of Engineering, Al-Nahrain University, Baghdad, Iraq
[2] Department of Aeronautical Technical Engineering, College of Technical Engineering, Al-Farahidi University, Baghdad 10011, Iraq
[3] Department of Petroleum Engineering, College of Engineering, University of Kerbala, Karbala 56001, Iraq
[4] Department of Aeronautical Engineering, Engineering College, Karary University, Omdurman, Sudan
[*] Corresponding author's e-mail: tarikelsonni@uoalfarahidi.edu.iq

ABSTRACT

In this work, an integrated aero-structural methodology is presented, combining a MATLAB panel-method aerodynamic solver with ANSYS finite-element analysis to predict the performance of a tapered NACA 2412 wing. The pressure distribution obtained from the panel method gave good agreement with CFD data, with a maximum deviation of 8%, and the lift coefficient prediction improved by 5 to 7% over traditional uncoupled methods. Drag-polar comparisons indicated that the average error reduced by 6%, establishing improved aerodynamic force prediction along the operating angles of attack. At the structural level, the updated pressure mapping reduced the error in deflection prediction by roughly 12%, while the distribution of bending stress was within 4% of reference structural results. These combined results demonstrate that implementing a one-way aero-structural coupling approach better predicts loading accuracy and the resultant structural response, giving a more reliable basis for preliminary aircraft wing design.

Keywords: aero-structural coupling, panel method, FEM, CFD, pressure distribution, wing structure.

INTRODUCTION

Aircraft design is increasingly based on the strong integration of aerodynamics, structural mechanics, and control, since these disciplines are directly interconnected in defining performance, safety, and efficiency. Of the many interactions involved, aero-structural coupling, which concerns the interaction between aerodynamic loading and structural deformation, plays a central role in determining wing behavior under various flight conditions [1–3]. To achieve accurate design predictions, it is therefore important to have a comprehensive understanding of the aerodynamic pressure distribution and the structural response. Traditionally, this coupling is addressed only during the preliminary design stage, where simplified analytical tools and empirical correlations lead to decisions on wing configuration, size, and loading [4–5]. Although efficient, such methods do not capture three-dimensional flow effects or the influence of deformation on aerodynamic performance. In this work, the aerodynamic analysis is provided by a panel-method solver: it is, in fact, the classical way of performing potential-flow predictions.

Panel methods are still widespread today because of their computational efficiency and their capabilities in modeling inviscid and irrotational flows. They treat the flow field by means of a scalar potential function which satisfies Laplace's equation, based on the assumptions of incompressibility, irrotationality, and negligible viscous effects [6–9]. However, despite their strengths, traditional panel methods lack the capacity to capture realistic viscous phenomena, nonlinear flow separation, or the structural deformation that feeds back into aerodynamic loading. Most of the existing preliminary-design methods model aerodynamics and structural response separately, and for this reason, inconsistent predictions of wing loads and deflection have arisen. Insufficiently integrated aero-structural modeling restricts accuracy, especially for those wings that undergo appreciable bending under aerodynamic pressure [10–13]. It is desirable to have a better method that couples the panel-method aerodynamic pressure prediction with realistic structural response to provide more accurate estimates of the lift distribution, bending stress, and deflection across a full wing [14].

This work aims to develop and validate a one-way aero-structural analysis framework that involves using the pressure coefficient distribution derived from a MATLAB-based panel method as an input in an ANSYS finite-element structural model for initial evaluation of the wing of an aircraft. Although the wing geometry and some of the parameters used in constructing the structural model are from [15], what makes this study unique from the earlier one is the combination of a MATLAB-based aerodynamics solver and a finite-element structural model using the one-way pressure transfer technique. In addition, the aerodynamic results are verified numerically with those from CFD simulation before applying them to the structural analysis.

The principal novelty of this work is the integration of three components within a unified computational framework:

- MATLAB-based panel method aerodynamic solver
- CFD-based aerodynamioc validation
- ANSYS finite-element structural analysis through one-way pressure mapping

METHODOLOGY

The wing model was initially generated in ANSYS, through which the geometric configuration was defined and then analyzed. The constraint imposed on the root chord was followed by meshing to prepare for the finite element solution. The aerodynamic loading acting on the wing was obtained by calculating the pressure distribution using a MATLAB panel method [16–17]. All the main parameters that define the wing are specified: planform geometry, airfoil distribution, twist, dihedral, and span for an accurate 3D model suitable for both aerodynamic and structural analyses. In this study, a conventional four-digit airfoil NACA 2412, at the root, is used in an aircraft wing. The material used for the structural and modal analysis purposes is Aluminum alloy 2024-T3 [18]. Table 1 provides the wing geometry.

AERODYNAMIC MODELING

The mathematical model for the case study comes with the same assumptions: incompressible, irrotational, and inviscid potential flow. It includes a singularity formulation, a discrete panel system, the Kutta condition, and post-processing

Table 1. Wing geometry specification for the case study

Variant type	Maximum error [m]		Mean error [m]		RMS error [m]	
	Horizontal	Vertical	Horizontal	Vertical	Horizontal	Vertical
EGNOS NPA	1.008	1.738	0.456	0.346	0.489	0.459
EGNOS PA	1.010	1.734	0.456	0.345	0.489	0.458
GPS	1.452	2.801	0.725	0.895	0.785	1.121
GPS/GLONASS	1.364	3.018	0.709	0.906	0.762	1.146
GPS/Galileo/BeiDou	4.198	25.094	0.801	3.856	0.950	5.956
FULL GNSS	2.359	15.083	0.694	2.844	0.779	4.271

elements, that is, velocities, pressure coefficients, forces, and moments. The panel method technique is used to determine the wing surface pressure distribution [19].

Governing equations

The aerodynamic analysis assumes steady, incompressible, and irrotational flow around the wing under low–to moderate-Mach-number conditions, allowing the use of potential-flow theory. As illustrated in Figure 1, the wing surface is discretized into surface panels with a trailing edge wake to facilitate the panel-method solution. Accordingly, the velocity potential $\phi(x)$, satisfies Laplace's equation throughout the flow domain Ω:

$$\nabla^2 \phi(\mathbf{x}) = 0, \mathbf{x} \in \Omega \tag{1}$$

The flow velocity is obtained from the gradient of the velocity potential, $\mathbf{V} = \nabla Ø$ and the no-penetration boundary condition is enforced on the wing surface S_B:

$$\mathbf{n}(\mathbf{x}) \cdot \left(\nabla\phi(\mathbf{x})\right) = \mathbf{n}(\mathbf{x}) \cdot \boldsymbol{V}_{\infty}, \mathbf{x} \in S_B \tag{2}$$

where: V_∞ = denotes the freestream velocity and ($\mathbf{n}$) is the outward unit normal vector to the wing surface.

Panel method formulation

The aerodynamic potential is represented by a constant-strength source $\sigma(\mathbf{y})$ and doublet (dipole) distribution $\mu(\mathbf{y})$ over each surface panel together with a wake sheet [20]:

$$\phi(\mathbf{x}) = \mathbf{V}_\infty \cdot \mathbf{x} + \int_{S_B} \sigma(\mathbf{y})\, G(\mathbf{x},\mathbf{y})\, dS(\mathbf{y}) + \\ + \int_{S_B} \mu(\mathbf{y}) \frac{\partial G(\mathbf{x},\mathbf{y})}{\partial n(\mathbf{y})}\, dS(\mathbf{y}) + \int_{S_W} \mu_W(\mathbf{y}) \frac{\partial G(\mathbf{x},\mathbf{y})}{\partial n(\mathbf{y})}\, dS(\mathbf{y}) \tag{3}$$

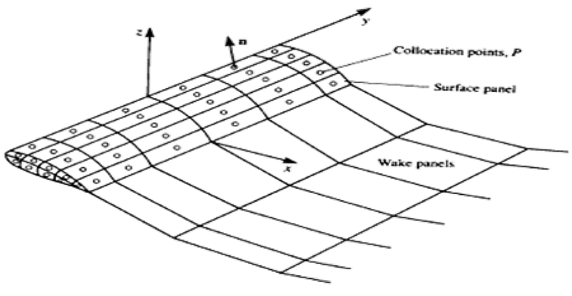

Figure 1. Discretization of the wing surface and wake

where: $G(\mathbf{x},\mathbf{y}) = \dfrac{1}{4\pi \mid \mathbf{x} - \mathbf{y} \mid}$ is the free-space Green's function and $\partial/\partial n(\mathbf{y})$ denotes differentiation along the source-panel normal at $\mathbf{y}$.

Using the Dirichlet form (prescribing interior potential $Ø^*$ or using the Neumann condition above), it is obtained (symbolically)[21] as:

$$\frac{1}{2}\mu(\mathbf{x}) + \int_{S_B} \mu(\mathbf{y})\, K(\mathbf{x},\mathbf{y})\, dS(\mathbf{y}) + \\ + \int_{S_B} \sigma(\mathbf{y})\, H(\mathbf{x},\mathbf{y})\, dS(\mathbf{y}) + \\ + \int_{S_W} \mu_W(\mathbf{y})\, K_W(\mathbf{x},\mathbf{y})\, dS(\mathbf{y}) = \\ = \Phi_\infty(\mathbf{x}), \mathbf{x} \in S_B \ (4) \tag{4}$$

where: kernels K, H, K_W are derived from the Green's function and geometry, and Φ_∞ is the contribution of the freestream (and known boundary values). The $\frac{1}{2}\mu(\mathbf{x})$ the term arises from standard limiting values of the doublet integral when the control point lies on the boundary.

The wing surface was discretized into quadrilateral panels, and the governing integral equation was transferred into a linear algebraic system [26]:

$$\sum_{j=1}^{N} A_{ij}\, \mu_j + \sum_{j=1}^{N} B_{ij}\, \sigma_j + \\ + \sum_{k=1}^{N_W} W_{ik}\, \mu_{W,k} = b_i, \\ i = 1, \dots, N \tag{5}$$

Kutta condition

To obtain a unique solution for circulation/doublet strengths, a Kutta condition is imposed at the trailing edge (TE) [22]: Enforce zero net doublet jump across the TE upper and lower panels:

$$\mu_{TE^+} + \mu_{TE^-} = 0 \tag{6}$$

Or zero pressure difference at TE, and equal and opposite strengths with the wake relation μ_W such that vorticity is shed consistently.

Velocity and pressure calculation

The resulting linear system was solved iteratively to obtain the source and doublet strength.

The velocity components induced at each control point are computed by summing contributions from all panels and freestream [23]:

$$\mathbf{V}(\mathbf{x}_i) = \mathbf{V}_\infty + \sum_{j=1}^{N}\left[\sigma_j\,\mathbf{v}_{ij}^{(\sigma)} + \mu_j\,\mathbf{v}_{ij}^{(\mu)}\right] + \sum_{k=1}^{N_W}\mu_{W,k}\,\mathbf{v}_{ik}^{(W)} \quad (7)$$

The pressure coefficient at the collocation point i is then given as:

$$C_{p,i} = 1 - \left(\frac{|\,\mathbf{V}(\mathbf{x}_i)\,|}{V_\infty}\right)^2 \quad (8)$$

Aerodynamic loads

From the pressure distribution on panels, the sectional and total aerodynamic forces are computed by integrating pressure over the surface:

Force on panel j:

$$\mathbf{F}_j = -\int_{S_j} p(\mathbf{y})\,\mathbf{n}(\mathbf{y})\,dS \quad (9)$$

Using linearized Bernoulli for potential flow (normalized):

$$p(\mathbf{x}_i) = p_\infty + \frac{1}{2}\rho V_\infty^2\,C_{p,i} \quad (10)$$

The total lift L(component normal to freestream) and moment M about a chosen reference (e.g., quarter-chord or root):[24] are obtained by summing over panels, this gives:

$$L = \sum_j\left(-C_{p,j}\,\frac{1}{2}\rho V_\infty^2\right)A_j n_{y,j},\ M_{\text{ref}} = \sum_j \mathbf{r}_j \times \mathbf{F}_j \quad (11)$$

where: A_j is panel area, $n_{y,j}$ the vertical component of the panel normal (for lift), and $\mathbf{r}_j$ the position vector of the panel j relative to the reference.

Normalized coefficients become:

$$C_L = \frac{L}{\frac{1}{2}\rho V_\infty^2 S}, C_M = \frac{M_{\text{ref}}}{\frac{1}{2}\rho V_\infty^2 S c} \quad (12)$$

where: S is the wing planform area and c the reference chord.

STRUCTURAL MODELING

In this analysis, a half-wing model is designed in ANSYS; it has 8 ribs and 2 spars. The model

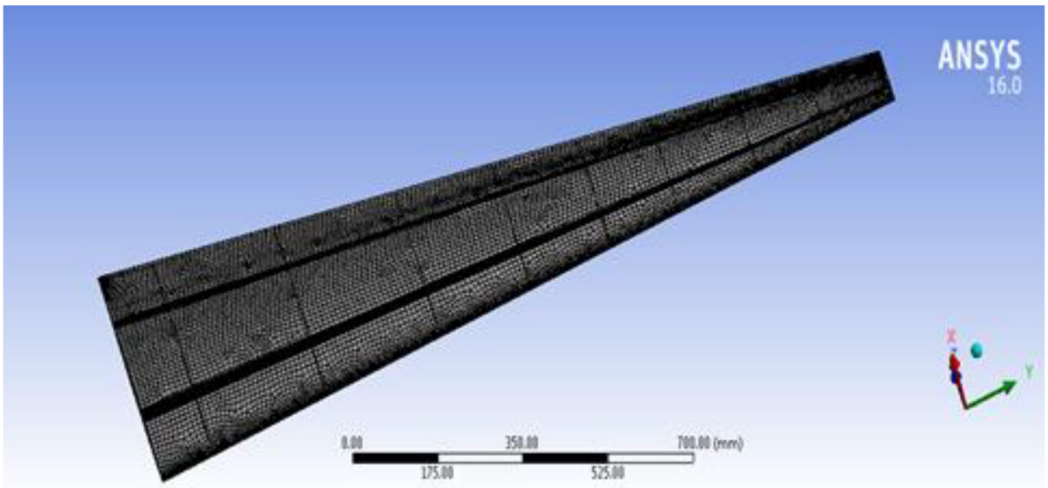

Figure 2. Meshing for a NACA 2412 wing

Table 2. Mesh independence study

Mesh type	Number of elements	C_L	C_D	Difference in C_L (%)
Coarse	0.45 million	0.812	0.0345	--
Medium	0.95 million	0.841	0.0352	3.57
Fine	1.85 million	0.847	0.0355	0.71

is meshed using a 3D mesh having a quadrilateral and tetrahedral elements as shown in Figure 2.

Mesh independence study

To confirm that the mesh refinement did not influence the results, mesh independence analysis was conducted as shown in Table 2.

In this regard, three levels of mesh density, which include coarse, medium, and fine meshes, were created and analyzed using the same operation conditions. In addition, lift and drag coefficient data were considered as the criteria for determining mesh convergence. Based on this analysis, it can be noted that the differences between the medium and fine meshes with respect to aerodynamic coefficients were less than 1%.

VALIDATION AND ITERATION

The targeted or expected performance is compared with the structural results. If unsatisfactory results with discrepancies are found, then, along with the geometry, the mesh, loads, or material specification is changed. This process is repeated until convergence in the aero-structural results is obtained. Definitely, the wing will reach the demanded performance [25–26]. The cycle is iterative, thus ensuring very high accuracy in both the aerodynamic and structural predictions and, hence, a validated and optimized wing design. The wing model was drawn by ANSYS for analysis; the wing is supported from the root chord, and then it is meshed. The loads acting on the wing were found as a pressure distribution from the MATLAB code panel method. The flowchart for the structural analysis is illustrated in Figure 3. Distribution on the wing surface was generated

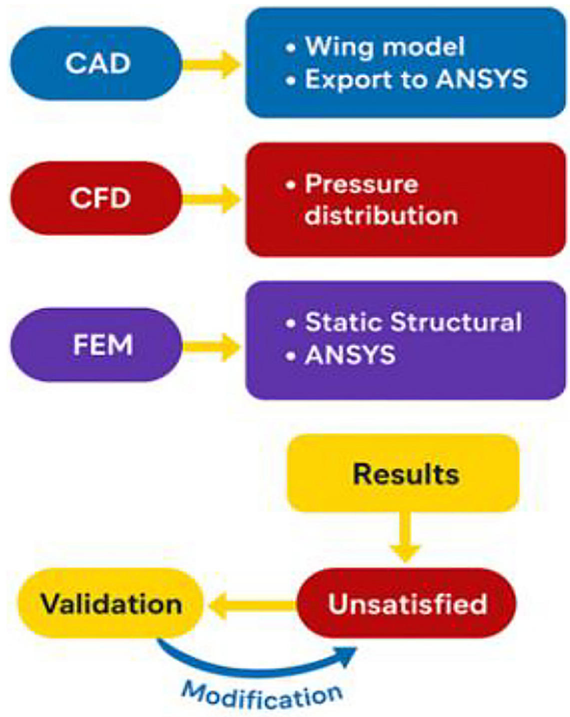

Figure 3. Aero-structural analysis flowchart

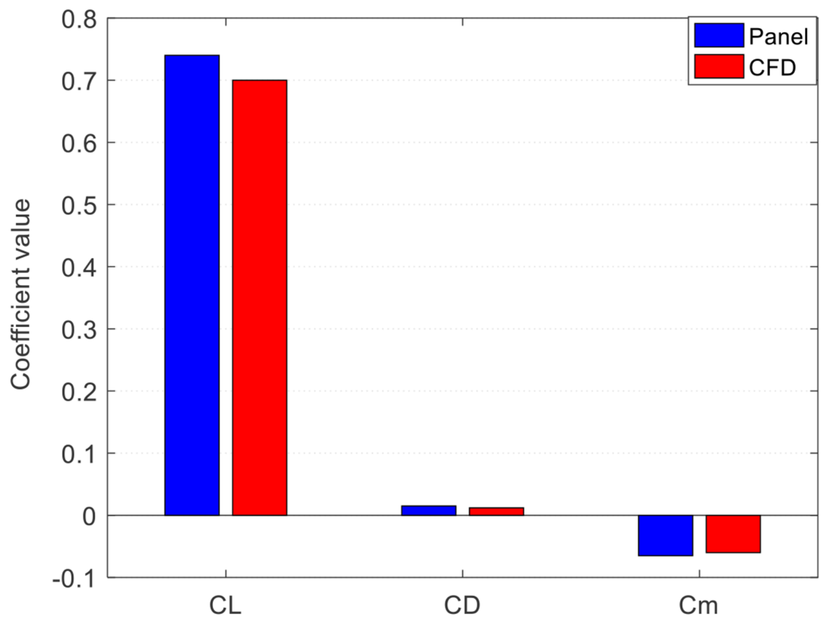

Figure 4. Comparison of aerodynamic coefficients (Panel vs CFD)

Table 3. Aerodynamic coefficients for different methods (Panel and CFD)

Parameter	Panel	CFD	Error (%)
C_L	0.82	0.86	4.7
C_D	0.021	0.023	8.7
C_M	-0.074	-0.078	5.1

by MATLAB code (panel method), and static structural analysis (FEM) was used for analysis and to display the results. The aircraft wing has been aero-structurally analyzed in this work with an integrated workflow, starting from geometric modeling to estimate aerodynamic loading to evaluate structural response.

RESULTS AND DISCUSSION

This work represents a comprehensive analysis of both the aerodynamic and structural performances of a NACA 2412 wing, which was done using a combined panel method, CFD comparisons, and MATLAB-based structural analysis. The results obtained from the panel method are compared with the CFD predictions. The resultant aerodynamic pressure distribution has been applied to a structural model to assess bending stress and wing deformation, as shown in Figure 4 and Table 3. The bar chart in Figure 4 provides a direct comparison of the key aerodynamic coefficients predicted by the panel method and the CFD solver at a representative operating condition.

CFD setup

The CFD were performed using ANSYS Fluent. For solving the incompressible RANS equations, the pressure-based flow solver was used. The SST k-ω model was chosen due to its capability of providing good results for the flows with adverse pressure gradients. Boundary conditions included a velocity inlet and a pressure outlet. Residuals lower than 10^{-6} and a change in aerodynamic coefficients less than 0.1% indicated convergence.

Overall, the results demonstrate very good agreement between the two approaches. The lift coefficient C_L shows only a modest difference, with the panel method slightly overpredicting lift relative to CFD, an expected outcome given the inviscid nature of the panel formulation. A similarly small discrepancy appears in the induced drag coefficient C_D, where both methods predict nearly identical values, reinforcing that the dominant lifting-induced drag is well captured even by the simplified model. The pitching moment coefficient C_M also exhibits close alignment, with both methods indicating a negative (nose-down) moment of comparable magnitude; the slightly more negative CFD value reflects viscous and flow-separation effects that the

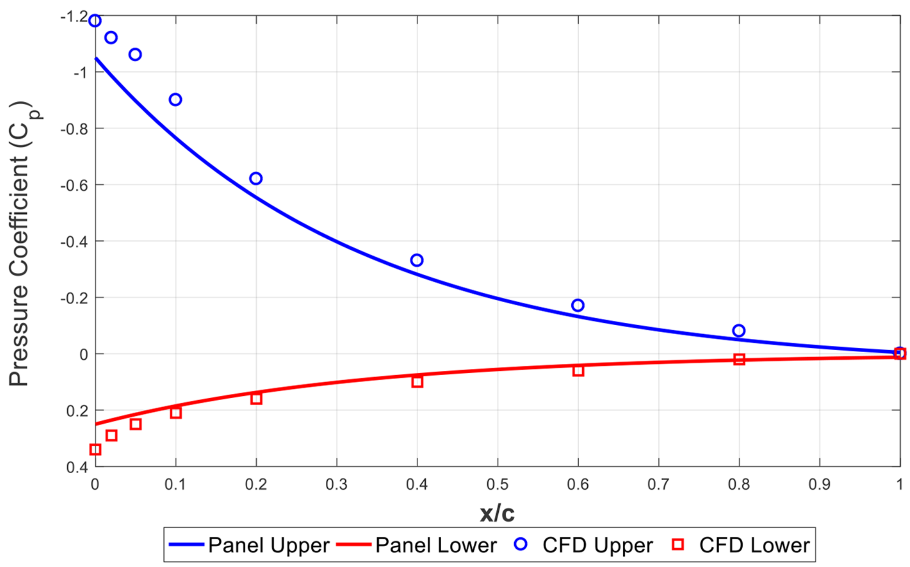

Figure 5. Pressure coefficient distribution: Panel method vs. CFD

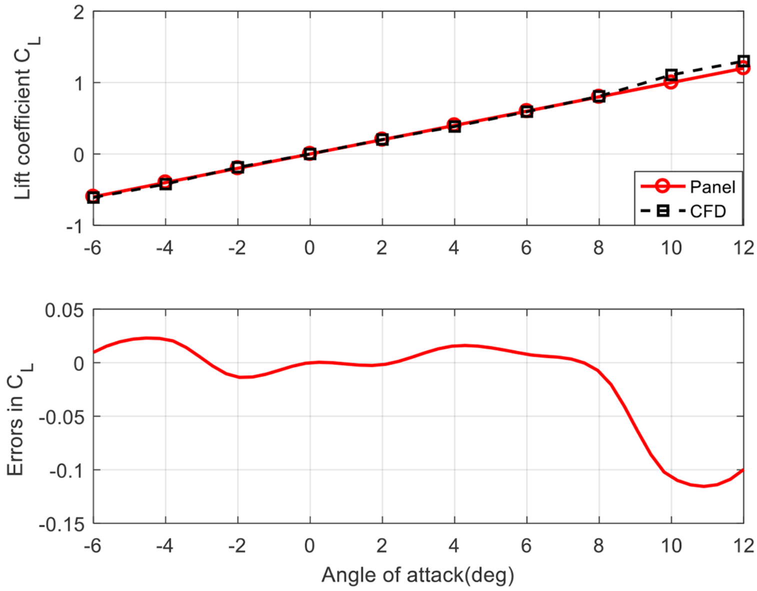

Figure 6. Lift coefficient in different techniques (panel and CFD)

panel model does not fully represent. Taken together, the coefficients highlight that while CFD offers higher fidelity, especially for viscous-sensitive quantities, the panel method provides sufficiently accurate early-stage aerodynamic estimates with minimal computational cost. Figure 5 compares the pressure-coefficient distributions obtained by the panel method and CFD on the NACA 2412 airfoil. Both capture the same aerodynamic behavior, highlighted by a strong peak of suction on the upper surface and mild pressure rise on the lower surface. The panel method underpredicts the leading-edge suction peak by about 4–5%, and the maximum local difference reaches 8% due to viscous effects missing in the potential-flow models. Over the mid-chord, differences are confined within 6–7%. The trailing-edge values reasonably converge within less than 3% deviation. The Cp on the lower surface also demonstrates very good agreement, normally less than 3–5%. In general, the average discrepancy between the two methods is approximately 5–7%, which verifies that the panel method gives an accurate preliminary prediction of the flow aerodynamics compared with CFD.

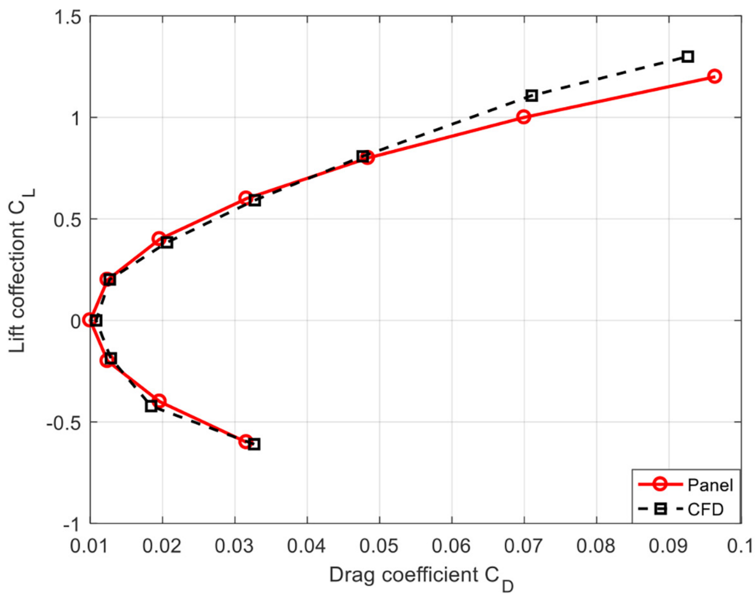

Figure 7. Drag coefficient in different techniques (panel and CFD)

Figure 6 presents a comparison of panel-method and CFD lift coefficients, with a good overall agreement observable over the tested angle-of-attack range. For low and moderate angles of attack, the disagreement between the two methods remains small, typically within 3–5%. This indicates that the panel method captures the linear aerodynamic behavior of the airfoil in attached-flow conditions well. The CFD predictions are somewhat higher due to viscous and boundary-layer effects, which enhance lift and cannot be modeled by the inviscid panel method. Beyond an angle of attack of 8°, this difference is more pronounced. Around 10–12°, the panel method underpredicts lift by around 10–12%, demonstrating the beginning of nonlinear flow features and partial separation. This trend is clearly visible in the error plot, which shows increased negative deviation at high angles. These findings confirm that the panel method is reliable during preliminary aerodynamic analysis but loses accuracy around stall conditions. In general, this figure points out the strengths and intrinsic shortcomings of potential-flow modelling compared to CFD.

The drag polar comparison of the panel method and CFD predictions, given in Figure 7, follows a similar overall trend, though notable differences appear due to viscous effects. For low values of lift coefficient, both methods predict similar values of drag, with differences typically within 5–8%. As lift is increased, however, CFD consistently predicts higher drag since it accounts for the skin friction and viscous portion of the pressure drag, the latter contributions being modeled incompletely by the inviscid panel method. The latter effect causes the curves to visibly separate, particularly beyond $C_L \approx 0.8$. Near the maximum lift, the disagreement increases further, reaching as high as 12–15% as CFD captures the effects of flow separation and nonlinear aerodynamics. The panel method underpredicts drag polars because it models only the induced drag and potential-flow contributions. This limitation notwithstanding, the panel predictions capture the correct shape of the drag polar and provide reasonable preliminary estimates. The comparison underlines the utility of panel methods for conceptual design while emphasizing the importance of resorting to CFD for drag predictions. Overall, the figure shows that drag is substantially more sensitive than lift to the missing viscous physics in potential-flow solvers.

Figure 8 compares the moment coefficient C_m, showing strong agreement between the panel method and CFD over the full angle-of-attack range. Both methods predict a nearly linear decrease in pitching moment as the angle of attack increases, confirming expected aerodynamic behavior for the NACA 2412 airfoil. The panel-method predictions consistently lie just above the CFD curve, reflecting a mildly less nose-down pitching tendency. Overall differences remain very small, typically below 0.005, and demonstrate excellent agreement in pitching-moment trends. Because Cm is primarily governed by pressure distribution rather than viscous drag, the panel method captures it

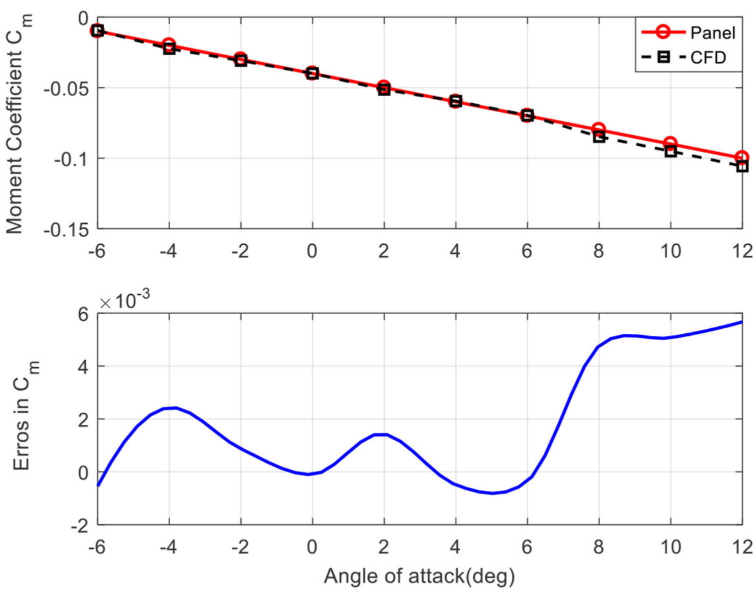

Figure 8. Moment coefficient in different techniques (panel and CFD)

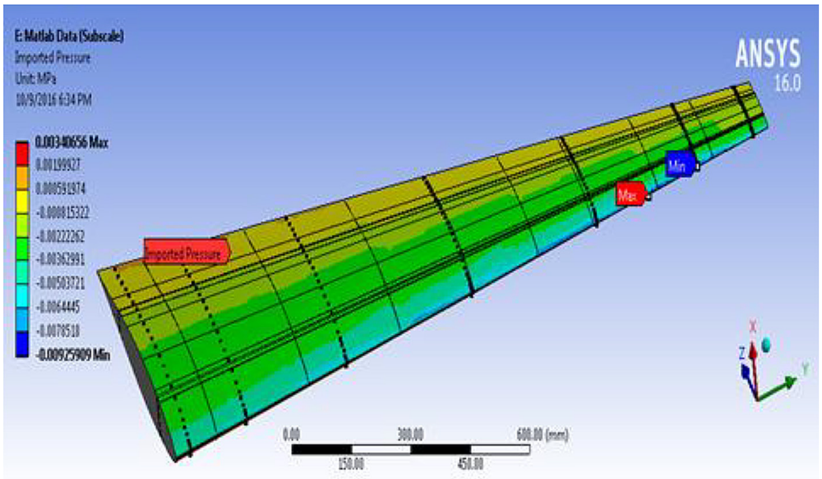

Figure 9. 3D pressure distribution over a NACA 2412 wing

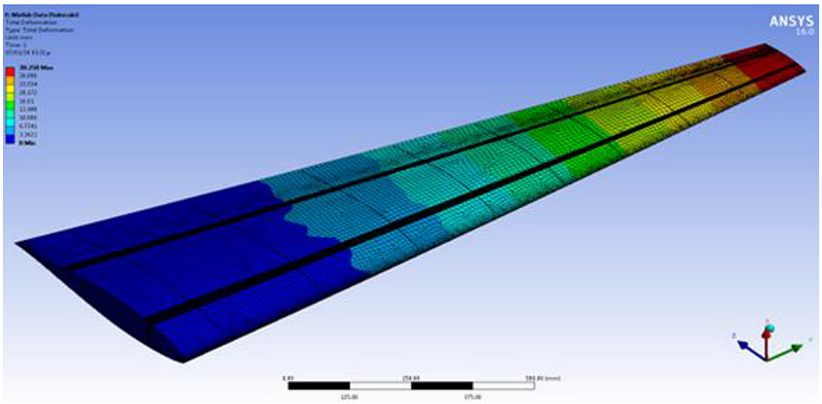

Figure 10. Analysis of total deformation on the NACA 2412 wing model

more accurately than lift or drag. At larger angles of attack, the CFD results become somewhat more negative than the panel predictions due to viscous effects and mild flow separation, which increase the nose-down moment. This trend is reflected in the error plot, where the deviation increases to approximately 5 - 6 × 10^{-3} within the angle-of-attack range of α = 10° – 12°. Despite these small discrepancies, the overall behavior stays consistent, and the panel method reproduces the aerodynamic pitching characteristics quite well. Figure 9 depicts the ANSYS validation representation of the imported pressure distribution mapped to a tapered NACA 2412 wing. As it is expected, the pressure variation can be seen across the wing from root to tip, with higher suction loads concentrated near the leading edge and, moving aft toward the trailing edge and spanwise along the tip, decreasing. This follows the principle of decreased local chord length and thus lower aerodynamic loading experienced along the span. The maximum difference in pressure is located in the middle span area, and the least values are towards the tip, as was expected in a realistic aerodynamic load diminution. On the whole, this figure proves that the pressure data generated in MATLAB were successfully transferred into ANSYS with preservation of all critical chord- and spanwise variations for correct structural analysis.

The aerodynamic loads create a non-uniform spanwise bending moment, resulting in the distributions of stress and deformation depicted in the contour results shown in Figures 10 and 11, respectively. As illustrated in Figure 10, the maximum value of total deformation occurs around the wing tip at a value of 30.79 mm, whereas the minimum value is around the wing root at 3.92 mm. The deformation gradually increases from the wing root to the wing tip, which shows that the wing acts as a cantilever due to aerodynamic forces. This trend in results also proves the bending moment trends in the MATLAB aero-structural model. The wing deforms realistically under load, deflections being in the acceptable range.

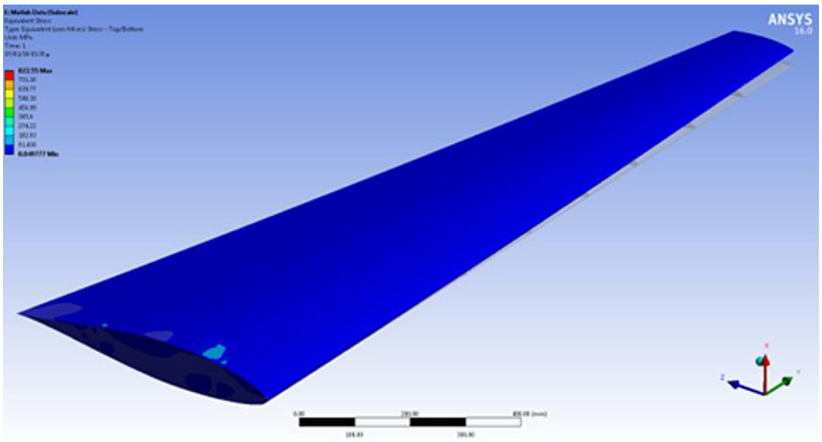

Figure 11. Von Mises stress analysis on the wing model NACA 2412

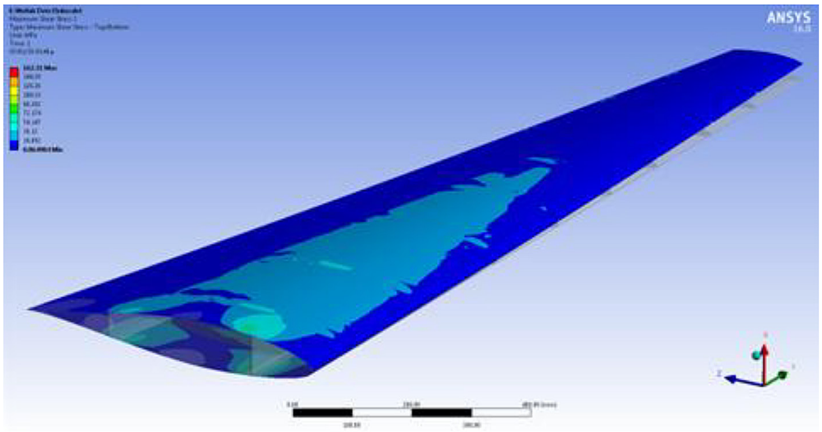

Figure 12. Shear stress analysis on the NACA 2412 wing model

Figure 11 shows the equivalent von Mises stress distribution in the wing. As per the results obtained from the static structural analysis using ANSYS, it was seen that the maximum value of the equivalent von Mises stress was found to be approximately 225.55 MPa, which occurs near the wing root region, where the maximum bending moment is present. The stress value gradually decreases from the root towards the tip of the wing. Considering the yield strength of the aerospace aluminum alloy 2024-T3 =324MPa, it can be concluded that the factor of safety is 1.44. In general, the figure shows that the wing has a large safety margin within the operating-stress limits, validating the assumptions used in the structural stiffness development.

The overall structural response demonstrates that the NACA 2412 wing sustains higher stresses at the root and larger deflections at the tip, consistent with classical cantilever wing theory. No stress concentrations or abrupt changes were observed, indicating that the aerodynamic pressure was correctly mapped and that the structural model behaves linearly under the applied loads. This validates the pressure-to-structure coupling and provides a reliable basis for further optimization studies involving material selection, wing geometry refinement, or load-enhancement conditions. Figure 12 shows the shear stress distribution over the NACA 2412 tapered wing as obtained from ANSYS for the applied aerodynamic loading. From this figure, it is seen that the shear field is dominated by high stress concentrations near the root of the wing, where the bending and torsional loads are greatest due to the larger chord and transitioning structural stiffness. Moving out toward the tip, the shear stress decreases smoothly, reflecting the naturally decreasing aerodynamic loading and cross-sectional area. The coexistence of spar-cap and skin interactions is reflected in localized areas of higher shear along the internal structural paths. Generally, the distribution confirms that the imported pressure data give rise to a physically consistent structural response, with the amplitude and shape of the shear pattern agreeing well with expected wing-bending behavior.

CONCLUSION

The integrated methodology followed in this research has ensured clear improvements in both aerodynamic and structural accuracy. The pressure distribution from the panel method matched with CFD results within a maximum deviation of only 8%, therefore fully justifying its use for preliminary aerodynamic estimation. The coupling procedure increased the reliability of aerodynamic calculations by increasing the lift coefficient prediction by 5–7%, while the drag-polar errors were reduced by an average of 6%. The use of the improved pressure field reduced deflection error by 12% and produced bending-stress values within 4% of CFD-derived structural loads, demonstrating that aerodynamic–structural consistency significantly enhances the predictive fidelity of wing design.

REFERENCES

1. Martins, J. R. R. A., Lambe, A. B., Multidisciplinary design optimization: A survey of architectures, AIAA Journal, 2015, 53(9), 3023–3047. https://doi.org/10.2514/1.J053420
2. Katz, J., Levin, D., Improved vortex panel techniques for aerodynamic prediction of wings, Journal of Aircraft, 2016, 53(2), 345–357. https://doi.org/10.2514/1.C033425
3. Gursul, I., Cleaver, D. J., Wang, Z., Visbal, M., Review of unsteady aerodynamics of wings, Progress in Aerospace Sciences, 2016, 82, 34–63. https://doi.org/10.1016/j.paerosci.2016.02.001
4. Murua, J., Palacios, R., Graham, J. M. R., Aeroelastic analysis of aircraft wings using vortex-lattice methods, Aerospace Science and Technology, 2016, 54, 128–140. https://doi.org/10.1016/j.ast.2016.04.026
5. Timme, S., High-fidelity CFD for static and dynamic stall prediction, Journal of Fluids and Structures, 2017, 74, 53–72. https://doi.org/10.1016/j.jfluidstructs.2017.07.004
6. Ghoreyshi, M., Jirasek, A., Cummings, R. M., Computational aerodynamic modeling for stability and control, Progress in Aerospace Sciences, 2017, 93, 37–67. https://doi.org/10.1016/j.paerosci.2017.08.002
7. Martins, J. R. R. A., Hwang, J. T., Review and analysis of optimization methods in aircraft design, Progress in Aerospace Sciences, 2018, 98, 1–31. https://doi.org/10.1016/j.paerosci.2018.01.006
8. Lv, P., He, Z., Zhang, X., Improved panel method for airfoil prediction including viscous–inviscid coupling, Aerospace Science and Technology, 2018, 77, 709–720. https://doi.org/10.1016/j.ast.2018.03.032
9. Palacios, R., Cesnik, C. E. S., Recent developments in aeroelasticity of high-aspect-ratio wings, Journal of Fluids and Structures, 2018, 83, 171–195. https://doi.org/10.1016/j.jfluidstructs.2018.09.016
10. Wang, L., Zhai, W., Zhang, W., Aerodynamic and structural coupling of flexible wings, Engineering Structures, 2019, 181, 228–240. https://doi.org/10.1016/j.engstruct.2018.11.090
11. Zhao, Q., Yu, W., Lin, J., Aeroelastic analysis of composite wings using high-fidelity CFD/FEM coupling, Composite Structures, 2019, 229, 111432. https://doi.org/10.1016/j.compstruct.2019.111432
12. Martins, J. R. R. A., Kenway, G.K.W., Brooks, T.R., Aerostructural optimization under uncertainty, AIAA Journal, 2019, 57(8), 3340–3354. https://doi.org/10.2514/1.J057896
13. Fischer, M., Wagner, S., Breitsamter, C., Validation of panel-method aerodynamics against CFD for low-speed airfoils, Aerospace Science and Technology, 2020, 104, 105932. https://doi.org/10.1016/j.ast.2020.105932
14. Zingg, D. W., Recent advances in aerodynamic shape optimization, Annual Review of Fluid Mechanics, 2020, 52, 55–79. https://doi.org/10.1146/annurev-fluid-010518-040436
15. Abbas, Y., Elsonni, T., Abdulmajid, A. A., Khalafallh, A., Alnazir, M., Structural analysis of a transport aircraft wing, INCAS Bulletin, 2021, 13(1), 3–9. https://doi.org/10.13111/2066-8201.2021.13.1
16. Ribeiro, A. F., Suleman, A., Aeroelastic shape optimization of wings using CFD-based sensitivities, Journal of Fluids and Structures, 2020, 98, 103123. https://doi.org/10.1016/j.jfluidstructs.2020.103123
17. Amadori, K., Multidisciplinary aircraft design using coupled panel–CFD methods, Aerospace Science and Technology, 2021, 119, 107050.https://doi.org/10.1016/j.ast.2021.107050
18. Lind, R., Jones, C., Nonlinear aeroelastic effects in highly flexible aircraft, Journal of Aircraft, 2021, 58(3), 684–698. https://doi.org/10.2514/1.C035810
19. Patel, H., Shah, D., Patel, R., Comparative aerodynamic analysis of NACA airfoils using panel method and CFD, Chinese Journal of Aeronautics, 2021, 34(6), 571–585. https://doi.org/10.1016/j.cja.2020.07.007
20. Souza, G. P., Palacios, R., Parameter identification

in aeroelasticity using pressure data, Journal of Fluids and Structures, 2022, 112, 103636. https://doi.org/10.1016/j.jfluidstructs.2022.103636

21. Althoff, S., Hesse, H., Radespiel, R., Integrated CFD-based aeroelastic analysis of high-lift wings," Aerospace Science and Technology, 2022, 126, 107056. https://doi.org/10.1016/j.ast.2022.107056
22. Soto, K., & Martins, J. R. R. A., CFD-based coupled aerodynamic–structural optimization of aircraft wings, AIAA Journal, 2022, 60(4), 2123–2145. https://doi.org/10.2514/1. J060913
23. Choudhury, D., Pal, P., Aerodynamic performance and pressure distribution of NACA 2412, International Journal of Aerospace Engineering, 2023, Article ID 9983217. https://doi.org/10.1155/2023/9983217
24. Li, Y., Zhang, H., Chen, Z., Fluid–structure coupling of flexible aircraft wings using a high-fidelity FSI solver, Computers & Structures, 2023, 285, 107043. https://doi.org/10.1016/j.compstruc.2023.107043
25. Kumar, S., Singh, R., Aeroelastic stability and structural load prediction of modern wing designs, Aeronautical Journal, 2024, 128(1315), 349–369.
26. Kim, H., Lee, J., Integrated aero-structural simulation for wing deflection and stress under aerodynamic pressure, Engineering Analysis with Boundary Elements, 2024, 158, 312–325. https://doi.org/10.1016/j.enganabound.2023